Journal of Power Sources 245 (2014) 371–376

Contents lists available at SciVerse ScienceDirect

Journal of Power Sources

journal homepage: www.elsevier.com/locate/jpowsour

Short communication

Electrochemical performance of $LiCoO_2/SrLi_2Ti_6O_{14}$ batteries for high-power applications

Jianhong Liu [a,b], Xiaoman Sun [b], Yanan Li [b], Xingqin Wang [b], Yun Gao [b], Ke Wu [b], Ningning Wu [b], Borong Wu [a,*]

[a] School of Chemical Engineering and Environment, Beijing Institute of Technology, Beijing 100081, China
[b] CITIC Guoan Mengguli Power Science and Technology Co., LTD, Beijing 102200, China

HIGHLIGHTS

- $LiCoO_2/SrLi_2Ti_6O_{14}$ batteries were designed and assembled for HEV application.
- The batteries exhibit high power performance and stable direct current resistance.
- Specific charge power density of 3973 W kg^{-1} was achieved at 50% depth of discharge.
- Electrochemical kinetics is performed to identify the excellent power performance.

ARTICLE INFO

Article history:
Received 12 May 2013
Received in revised form
10 June 2013
Accepted 26 June 2013
Available online 5 July 2013

Keywords:
Hybrid electric vehicle
Power performance
Li diffusion capability
Electronic conductivity

ABSTRACT

$LiCoO_2/SrLi_2Ti_6O_{14}$ Li-ion rechargeable batteries with ~6 Ah capacities are designed and assembled for use in hybrid electric vehicle (HEV) applications. For comparison, $LiCoO_2/Li_4Ti_5O_{12}$ batteries are also constructed using similar processing parameters. Power tests are carried out using the hybrid pulse power characterization (HPPC) method. Experimental results show that the $LiCoO_2/SrLi_2Ti_6O_{14}$ batteries have better power performance and more stable charge/discharge direct current (DC) resistances compared with the $LiCoO_2/Li_4Ti_5O_{12}$ batteries. At a 50% depth of discharge (DOD), $LiCoO_2/SrLi_2Ti_6O_{14}$ batteries have an excellent specific charge power density of 3973 W kg^{-1}, which can be attributed to the high Li diffusion capability and high electronic conductivity of the $SrLi_2Ti_6O_{14}$ material.

1. Introduction

Safety and cycling life are important concerns for high-capacity Li-ion batteries used in electric vehicles and energy storage applications. Thus, the spinel $Li_4Ti_5O_{12}$ has gained significant attention because of its improved safety and cycling properties over carbon-based anodes. These advantages include the zero-strain characterization during Li-ion intercalation/de-intercalation, higher operation potential (above the potential of the solid electrolyte interface (SEI) layer formation), and safer overcharging behavior [1–7].

However, the lower operating voltage of lithium-ion batteries using $Li_4Ti_5O_{12}$ as the anode leads to a large decrease in energy density for Li-ion batteries, as well as shorter endurance mileage compared to carbon-based anodes when used in electric vehicles [8]. In addition, when producing Li-ion batteries it is difficult to increase the volume energy density by increasing the coating content of the active material on the current collector. This difficulty is caused by the large specific surface area and lower tap density of $Li_4Ti_5O_{12}$.

$SrLi_2Ti_6O_{14}$, which has a theoretical capacity of 262 mAh g^{-1} [9], possesses a three-dimensional structure with the *Cmca* space group in which Li ions can migrate quickly because of the structure's high diffusion coefficient, allowing for excellent high-drain performance. Belharouak et al. reported that an $SrLi_2Ti_6O_{14}$ electrode had lower area specific impedance (ASI) than a $Li_4Ti_5O_{12}$ electrode [10]. Dambournet et al. reported measuring a 92 mAh g^{-1} capacity for an $SrLi_2Ti_6O_{14}$ electrode at an approximate rate of 8C; this capacity was about 83.6% of its 1C capacity, exhibiting excellent rate performance [9]. Thus, $SrLi_2Ti_6O_{14}$ was considered to be a potential replacement for $Li_4Ti_5O_{12}$ because of its lower operating voltage (~1.40 V vs. Li^+/Li), lower ASI, and higher tap density, allowing for

* Corresponding author. Tel./fax: +86 010 89702984.
E-mail addresses: ljhmgl@aliyun.com, wubr@bit.edu.cn (B. Wu).

0378-7753/$ – see front matter © 2013 Elsevier B.V. All rights reserved.
http://dx.doi.org/10.1016/j.jpowsour.2013.06.149

the possibility of a higher energy density while maintaining good power performance [11]. To our knowledge, there have been no reports using $SrLi_2Ti_6O_{14}$ as an anode in Li-ion batteries designed for hybrid electric vehicle applications.

In this work, batteries for HEV applications with ~6 Ah capacities were designed and assembled using either $SrLi_2Ti_6O_{14}$ or $Li_4Ti_5O_{12}$ as the anode. The electrochemical performance of the two kinds of batteries was investigated, focusing on the power performance; the differences in those results are discussed in this paper.

2. Experimental

2.1. Battery assembly and power performance test

Li-ion batteries with 6 Ah capacities designed for HEV applications were constructed using $LiCoO_2$ as the cathode and $SrLi_2Ti_6O_{14}$ (provided by MGL Co. Ltd., China) as the anode. The proportion of active material in the anode electrode was a 92% mass fraction. The $SrLi_2Ti_6O_{14}$ coating content on the current collector was about 210 g m^{-2}. The electrolyte was 1 mol L^{-1} $LiPF_6$ in ethylene carbonate/dimethyl carbonate/ethyl–methyl carbonate mixtures (1:1:1, V/V), and the separator was UPZS40 (UBE, Japan). A lamination-type battery was constructed, as shown in Fig. 1. The assembled batteries were somewhat cathode limited (3% capacity excess of the anode relative to cathode). For comparison, $Li_4Ti_5O_{12}$ was purchased from a vender (BTR Co. Ltd., China) and used as the anode material to assemble $LiCoO_2/Li_4Ti_5O_{12}$ full cells with the same anode electrode formula, electrolyte, membrane, and cathode as the $LiCoO_2/SrLi_2Ti_6O_{14}$ batteries. The actual reversible specific capacities (vs. Li^+/Li in half-cell) of the $LiCoO_2$, $Li_4Ti_5O_{12}$ and $SrLi_2Ti_6O_{14}$ in this work are 164 mAh g^{-1}, 172 mAh g^{-1} and 124.3 mAh g^{-1}, respectively. Because the stable reversible capacity of $SrLi_2Ti_6O_{14}$ is about two-thirds that of $Li_4Ti_5O_{12}$ [9], the specific coating content of the $SrLi_2Ti_6O_{14}$ electrode on the current collector was approximately 1.5 times that of the $Li_4Ti_5O_{12}$ electrode. After a roll-pressing process, the final electrode thickness of $SrLi_2Ti_6O_{14}$ and $Li_4Ti_5O_{12}$ are 95 μm and 73 μm, respectively. The other processing parameters were similar for the two anode materials.

The batteries were first charged to 3.2 V for the $LiCoO_2/SrLi_2Ti_6O_{14}$ batteries and 2.8 V for the $LiCoO_2/Li_4Ti_5O_{12}$ batteries at a 0.1C rate, and were then discharged to 1.5 V at a 0.1C rate at 25 °C. After degassing and a final sealing operation, the batteries were charged and discharged three times at a 1.0C rate at room temperature for the following power test.

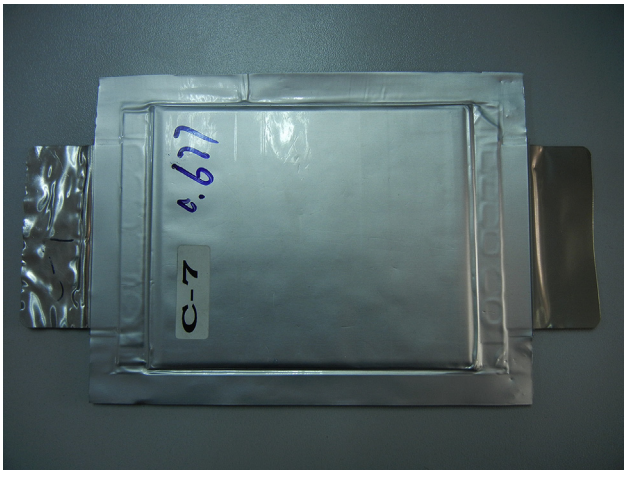

Fig. 1. Experimental pouch battery with 6 Ah capacities, designed for power applications.

Power comparison tests were performed on the batteries at room temperature according to the hybrid pulse power characterization (HPPC) method [12]. The power test was carried out using high-power charge–discharge equipment (BT2000, 5V-300A, Arbin, USA).

2.2. Electrochemical characterization of materials

The electronic conductivity of the $SrLi_2Ti_6O_{14}$ and $Li_4Ti_5O_{12}$ powders were carried out on a conductivity meter (Shanghai SB118, China) using a conventional four-point probe method at room temperature. The specific surface areas of the two powders were measured on a Gemini2360 instrument (Micromeritics, USA) using an N_2 adsorption-desorption process at 77 K. The tap density of each material was examined using a tapping apparatus (FZS4-4B, IRsID, China). X-ray diffraction patterns of powders were collected on a Bruker D8 ADVANCE Powder Diffractometer with Cu Kα radiation (λ = 1.5406 Å) between 10 and 90° (40 kV, 40 mA, step size = 0.02° and a count time = 0.2 s/step.). Molar volume data of powders were deduced from Rietveld refinements, which were performed using Bruker Topas4.2 software.

Electrodes used for half-cells, were made by casting a slurry of 90 wt.% active material oxide, 5 wt.% conductive reagent (Timcal, super-P), and 5 wt.% PVDF binder (Kynar, ARKEMA) in a *N*-methyl-2-pyrollidinone (NMP) solvent onto a Cu-foil substrate. The slurry was cast using a doctor blade. The cast laminates were dried in air at 120 °C for 2 h and then in a vacuum at 70 °C for 8 h. The electrodes were then pressed to fixed thicknesses of 35–40 μm. Lithium coin cells (CR2032) were fabricated in an Ar-filled glove box (<1 ppm O_2, MBraun, Germany). Lithium metal was used as the counter electrode, a Celgard 2400 microporous polypropylene membrane as the separator, and 1 M $LiPF_6$ in a 1:1:1 volume fraction of ethylene carbonate (EC)/dimethyl carbonate (DMC)/ethylmethyl carbonate (EMC) as the electrolyte. Charge–discharge formation and galvanostatic intermittent titration technique (GITT) experiments were performed on a multichannel potentiostatic–galvanostatic system (CT2010A, Land, China). For the GITT measurement, the coin cells were charged and discharged with a constant current flux for a given time followed by an open-circuit stand for a specified time interval.

3. Results and discussion

3.1. Electrochemical performance of full cells

Fig. 2 shows the charge–discharge curves for the full cells, which were designed for HEV applications; each used $SrLi_2Ti_6O_{14}$ or $Li_4Ti_5O_{12}$ as its anode. The basic parameters of the batteries are listed in Table 1. Fig. 2 shows that the $LiCoO_2/SrLi_2Ti_6O_{14}$ battery curves have a higher voltage plateau than the $LiCoO_2/Li_4Ti_5O_{12}$ batteries, resulting in greater energy storage at the same capacity. Because of the lower reversible capacity of $SrLi_2Ti_6O_{14}$ compared with $Li_4Ti_5O_{12}$, more active material ($SrLi_2Ti_6O_{14}$) was used in the $LiCoO_2/SrLi_2Ti_6O_{14}$ batteries for designs of the same capacity as $LiCoO_2/Li_4Ti_5O_{12}$ batteries. This addition causes the $LiCoO_2/SrLi_2Ti_6O_{14}$ battery to weigh more than the $LiCoO_2/Li_4Ti_5O_{12}$ battery. However, because of the higher operating voltage of the $LiCoO_2/SrLi_2Ti_6O_{14}$ batteries, as shown in Fig. 2 and Table 1, they had higher energy densities than the $LiCoO_2/Li_4Ti_5O_{12}$ batteries.

Fig. 3 shows the rate curves for the two kinds of batteries. Their 25C rate discharge capacity ratios are close to each other. In contrast, the charge capacity ratios of the two kinds of batteries are very different; at a 15C rate they have 88.3% and 63.6% of the 1.0C capacity for the $LiCoO_2/SrLi_2Ti_6O_{14}$ and $LiCoO_2/Li_4Ti_5O_{12}$ batteries, respectively. The fast-charge performance of the $LiCoO_2/SrLi_2Ti_6O_{14}$

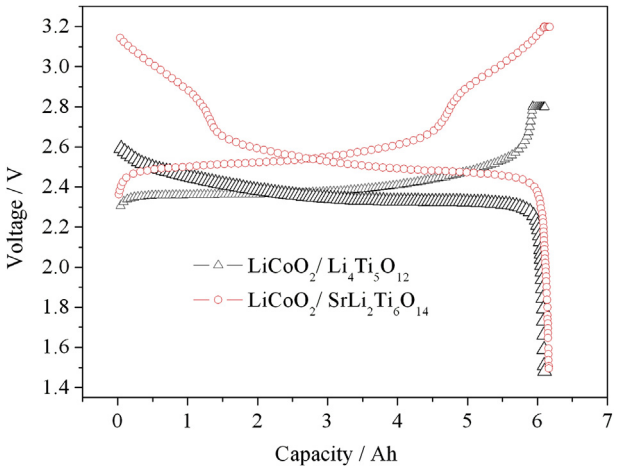

Fig. 2. Two kinds of full cell charge–discharge curves obtained at a 1.0C rate.

Table 1
The basic parameters of the two kinds of full cells.

Battery system	Capacity of cells (Ah)	Weight of cells (g)	Mean voltage in the discharge (V)	Energy density (Wh kg^{-1})
$LiCoO_2/Li_4Ti_5O_{12}$	6.10	255.13	2.37	56.71
$LiCoO_2/SrLi_2Ti_6O_{14}$	6.16	276.30	2.60	57.97

batteries is beneficial for HEV applications or special electric vehicles, which need to be fully charged in very short times.

The common rate test only reflects the charge or discharge performance at a known large current. However, the power input or output of batteries is dynamic and changes with the state of charge (SOC) or depth of discharge (DOD). For a comprehensive power comparison between the two kinds of batteries, the HPPC test method was introduced in this work. The objective of the HPPC test is to measure the discharge pulse and regen pulse power as functions of the DOD. A constant current mode was used with the characterization profile shown in Fig. 4. The test is made up of repetitions of this profile, with intervals of a 10% DOD constant current discharge section, each followed by 1 h rest period to allow the cell to return to electrochemical and thermal equilibrium before applying the next pulse profile.

Fig. 5 shows the specific power density as a function of the DOD for the two kinds of batteries. The rate of discharge pulse current is 10C ($I = 60$ A), and the rate of charge pulse current is 7.5C ($I = 45$ A). During the entire discharge process of the $LiCoO_2/SrLi_2Ti_6O_{14}$ batteries, the charging power stays high as the DOD increases, as shown in Fig. 5(a). Between 30% and 80% DOD, the $LiCoO_2/SrLi_2Ti_6O_{14}$ batteries had higher power densities than the $LiCoO_2/Li_4Ti_5O_{12}$ batteries in both the charge and discharge processes. If the lower limit of the power application is set to 2500 Wh kg^{-1}, the usage range of the $LiCoO_2/SrLi_2Ti_6O_{14}$ batteries (about 30–80% DOD) is larger than the range of the $LiCoO_2/Li_4Ti_5O_{12}$ batteries (about 40–60% DOD). The wider DOD range of the $LiCoO_2/SrLi_2Ti_6O_{14}$ batteries can raise utilization efficiency in applications. As shown in Table 2, at 50% DOD the $LiCoO_2/SrLi_2Ti_6O_{14}$ battery had a specific power density of 3973 W kg^{-1}, much higher than 2634 W kg^{-1} for the $LiCoO_2/Li_4Ti_5O_{12}$ battery. This high charging power can improve the energy regeneration efficiency for batteries in HEV applications or in some special bus applications. Additionally, energy density and power density restrict each other when practically designing Li-ion batteries. Thus, by matching the power performance of $LiCoO_2/SrLi_2Ti_6O_{14}$ batteries with $LiCoO_2/Li_4Ti_5O_{12}$ batteries, a higher energy density can be achieved than previously possible.

Usually, the direct current (DC) impedance of Li-ion batteries during charge or discharge changes dynamically. The dynamic DC impedance is important for designing battery management systems (BMSs). The discharge and regen DC resistances are calculated using a $\Delta V/\Delta I$ formula for each iteration of the test profile in accordance with Fig. 4, eq. (1), and eq. (2) [12].

$$\text{Discharge Resistance} = \frac{\Delta V_{\text{discharge}}}{\Delta I_{\text{discharge}}} = \frac{V_{t1} - V_{t0}}{-(I_{t1} - I_{to})} = \frac{V_{t1} - V_{t0}}{I_{t0} - I_{t1}} \quad (1)$$

$$\text{Regen Resistance} = \frac{\Delta V_{\text{regen}}}{\Delta I_{\text{regen}}} = \frac{V_{t3} - V_{t2}}{-(I_{t3} - I_{t2})} = \frac{V_{t3} - V_{t2}}{I_{t2} - I_{t3}} \quad (2)$$

Fig. 6 shows the DC resistance of the two kinds of batteries as a function of the DOD. In nearly the entire DOD range, the DC resistance in the $LiCoO_2/SrLi_2Ti_6O_{14}$ system remains nearly the same between the charge and discharge processes. In contrast, the $LiCoO_2/Li_4Ti_5O_{12}$ system DC resistance is different for the charge and discharge processes. The relatively stable DC resistance of the $LiCoO_2/SrLi_2Ti_6O_{14}$ system is favorable for BMS design in HEV applications. As shown in Fig. 6(a), for the first 20% of the DOD there is one inflection point (indicating the point of largest kinetic impedance) for the $LiCoO_2/SrLi_2Ti_6O_{14}$ batteries, which differs from the $LiCoO_2/Li_4Ti_5O_{12}$ batteries. Using integrative analysis with a similar inflection point shown in Fig. 5(a) at 20% DOD, we speculate a relationship with multiple plateau characterization of the

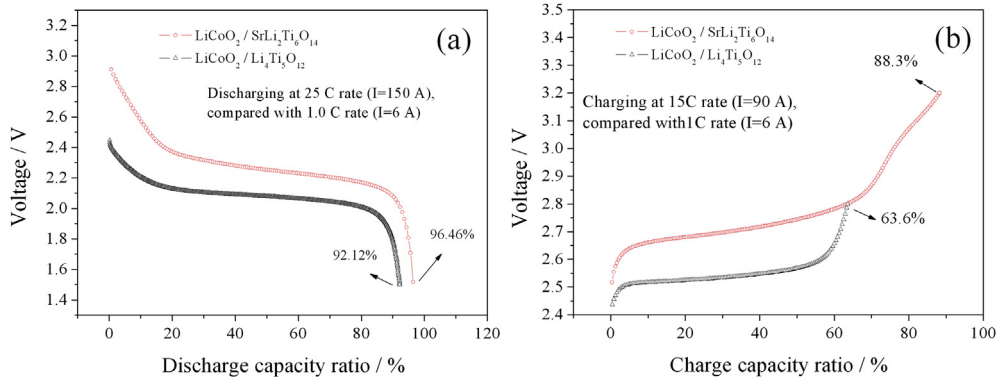

Fig. 3. Rate-performance comparison of the two kinds of batteries based on (a) discharge rate and (b) charge rate.

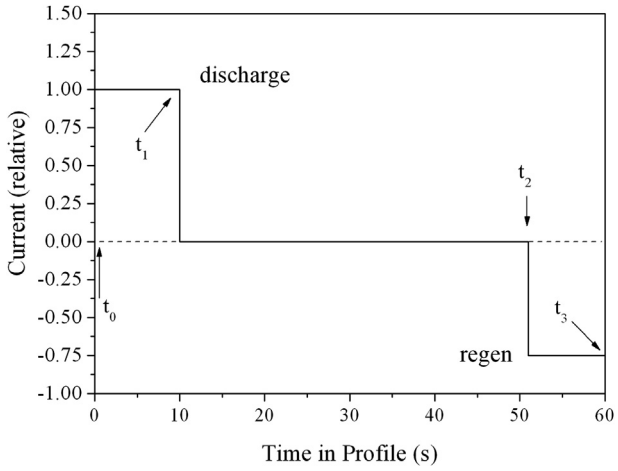

Fig. 4. Hybrid pulse power characterization test profile [12].

$SrLi_2Ti_6O_{14}$ electrode during lithium intercalation/de-intercalation. This DC resistance inflection point corresponds to a ~2.8 V platform position during the charge–discharge process for $LiCoO_2$/$SrLi_2Ti_6O_{14}$ batteries, as shown in Fig. 2.

3.2. Electrochemical kinetics discussion

In this section we explore how the $LiCoO_2$/$SrLi_2Ti_6O_{14}$ batteries have excellent power properties. Belharouak et al. demonstrated the outstanding power performance of an $SrLi_2Ti_6O_{14}$ electrode using the area specific impedance (ASI) method; they proposed that $SrLi_2Ti_6O_{14}$ may have a high electronic conductivity because of its multivalent character during the electrochemical reaction process [10]. Dambournet et al. proposed that its excellent power performance was caused by the presence of a special 3D network with voids suitable for Li migration [9]. However, no studies have reported electronic conductivity data for $SrLi_2Ti_6O_{14}$ or the Li-ion migration kinetic properties in $SrLi_2Ti_6O_{14}$ particulate material during the charge–discharge process.

The electronic conductivities of the powders are listed in Table 3. The electronic conductivity detection limit of the instrument used in our study is about $\sim 10^{-9}$ S cm^{-1}. The electronic conductivity of commercial $Li_4Ti_5O_{12}$ was below the limit of detection, which indicated that the electronic conductivity was $<10^{-9}$ S cm^{-1}. The electronic conductivity of the $SrLi_2Ti_6O_{14}$ powder was 3.63×10^{-7} S cm^{-1}, which is at least two orders of magnitude higher than that for the $Li_4Ti_5O_{12}$ powder. This difference indicates that $SrLi_2Ti_6O_{14}$ has a smaller electrical resistance during the electrochemical reaction.

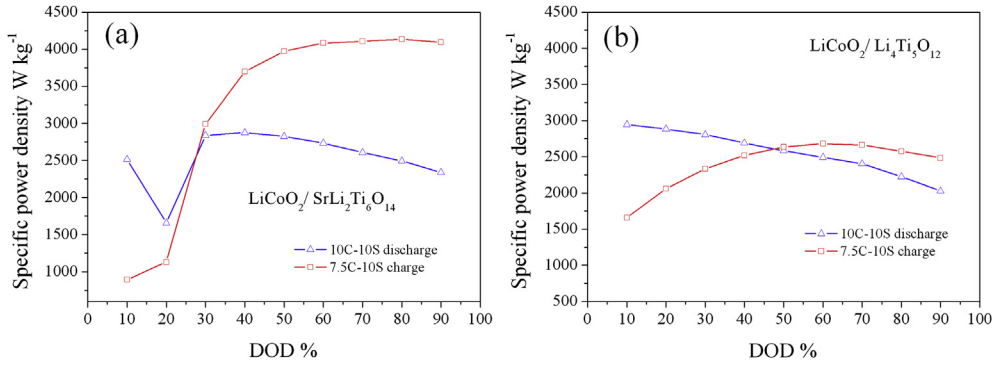

Fig. 5. Specific power density as a function of DOD in HPPC tests for (a) $LiCoO_2$/$SrLi_2Ti_6O_{14}$ battery and (b) $LiCoO_2$/$Li_4Ti_5O_{12}$ battery.

Table 2
Power and DC resistance data obtained at 50% DOD using the HPPC method.

Battery system	Discharge DC resistance (mΩ)	Specific discharge power density (W kg^{-1})	Charge DC resistance (mΩ)	Specific charge power density (W kg^{-1})
$LiCoO_2$/$Li_4Ti_5O_{12}$	1.97	2583	1.84	2634
$LiCoO_2$/$SrLi_2Ti_6O_{14}$	1.98	2826	1.92	3974

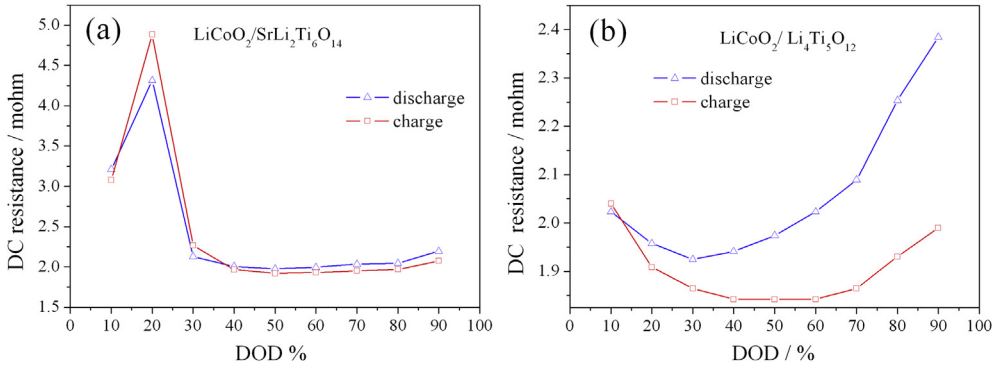

Fig. 6. Direct current (DC) resistance of the two kinds of batteries: (a) $LiCoO_2$/$SrLi_2Ti_6O_{14}$ and (b) $LiCoO_2$/$Li_4Ti_5O_{12}$.

Table 3
Physical parameters of $SrLi_2Ti_6O_{14}$ and $Li_4Ti_5O_{12}$ powders.

Powder	Tap density (g cm^{-3})	Specific surface area (m^2 g^{-1})	Electronic conductivity (S cm^{-1})	Lattice parameters		
				a (Å)	*b* (Å)	*c* (Å)
$Li_4Ti_5O_{12}$	0.97	4.23	$<10^{-9}$	8.3601	8.3601	8.3601
$SrLi_2Ti_6O_{14}$	1.42	0.83	3.63×10^{-7}	16.5742	11.1553	11.4771

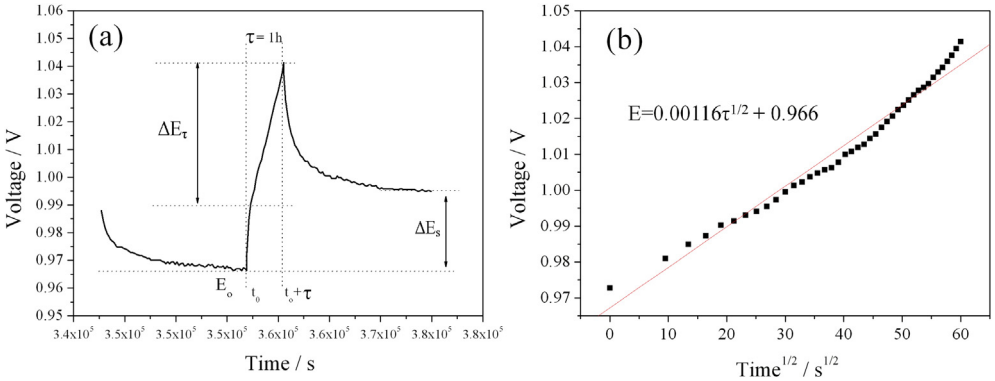

Fig. 7. (a) τ vs. E profile of an $SrLi_2Ti_6O_{14}$/Li coin cell for a single GITT titration. (b) Relationship of the $SrLi_2Ti_6O_{14}$/Li cell voltage as a function of $\tau^{1/2}$ for one titration.

To further compare the kinetics of the lithium ion extraction and insertion reaction in the $Li_4Ti_5O_{12}$ and $SrLi_2Ti_6O_{14}$ electrodes and to quantize the lithium ion transfer speed inside the material, the chemical diffusion coefficient of the lithium ion (D_{Li^+}) in the active material is used in this work. The chemical diffusion coefficient of a lithium ion is an important kinetic parameter for lithium-ion insertion and extraction reactions in intercalation materials. Based on chronopotentiometry at near-thermodynamic-equilibrium conditions, galvanostatic intermittent titration (GITT) is a reliable method to determine D_{Li^+}. Based on the GITT measurement, the chemical diffusion coefficient of Li^+ can be calculated by the following equation [13–18]:

$$D_{Li^+} = \frac{4}{\pi}\left(\frac{m_B V_M}{M_B S}\right)^2 \left(\frac{\Delta E_s}{\tau \mathrm{d}E_x/\mathrm{d}\sqrt{\tau}}\right)^2 \quad \left(\tau << L^2/D_{Li^+}\right) \tag{3}$$

where V_M is the molar volume of $SrLi_2Ti_6O_{14}$ or $Li_4Ti_5O_{12}$: 159.36 cm^3 mol^{-1} or 43.99 cm^3 mol^{-1}, respectively, deduced from crystallographic data; M_B and m_B are the molecular weight and

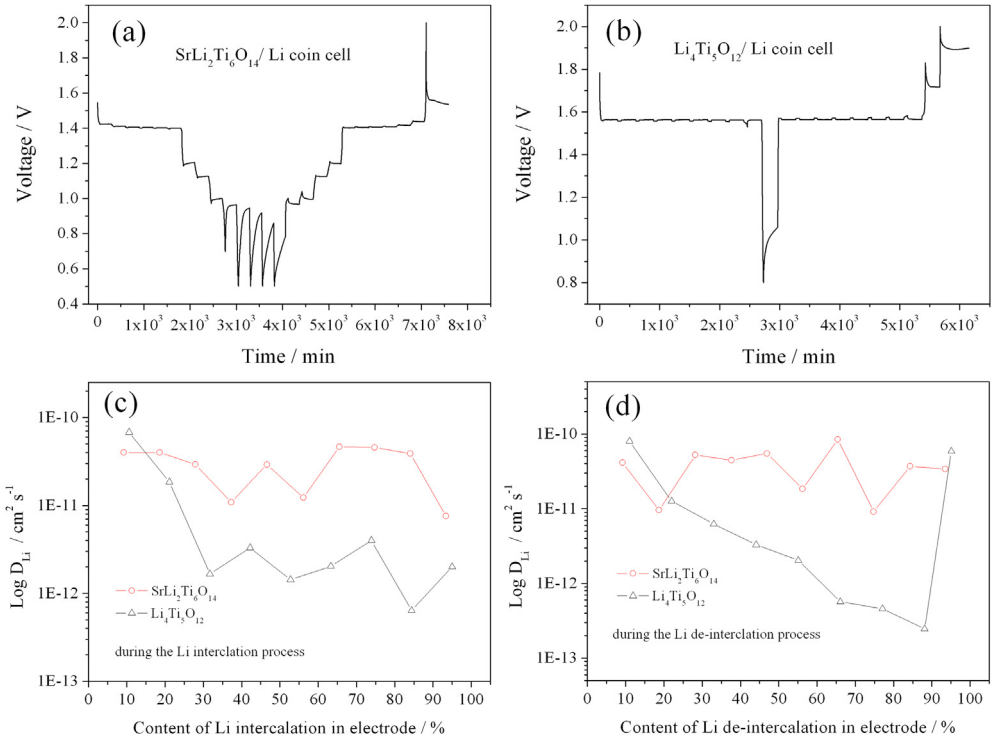

Fig. 8. Li-ion diffusion coefficient for $SrLi_2Ti_6O_{14}$ and $Li_4Ti_5O_{12}$ obtained by GITT: (a) GITT curve of $SrLi_2Ti_6O_{14}$, (b) GITT curve of $Li_4Ti_5O_{12}$, (c) log(D_{Li}) as a function of the Li intercalation content, and (d) log(D_{Li}) as a function of the Li de-intercalation content. The active material mass for the coin cells is about 3.6 mg.

mass of the active material, respectively; S is the active surface area of the electrode, deduced from BET testing; and L is the thickness of the electrode. If the E versus $\tau^{1/2}$ behavior is linear, as shown in Fig. 7(b), then eq. (3) can be simplified to the following [13,14]:

$$D_{Li^+} = \frac{4}{\pi}\left(\frac{m_B V_M}{M_B S}\right)^2 \left(\frac{\Delta E_s}{\Delta E_t}\right)^2 \quad (4)$$

Usually, to obtain the steady state cell voltage, a small current flux and long time interval should be used for the GITT test. In this work, the GITT data were collected at a 0.1C rate ($\sim$13 mA g^{-1} for $SrLi_2Ti_6O_{14}$ and $\sim$17 mA g^{-1} for $Li_4Ti_5O_{12}$) and a time interval of 240 min. Fig. 8 shows the variation of the lithium ion diffusion coefficient (D_{Li^+}) as a function of the Li intercalation/de-intercalation content during the second charge–discharge process for the $SrLi_2Ti_6O_{14}$/Li and $Li_4Ti_5O_{12}$/Li coin cells. Fig. 8(c) and (d) shows that the D_{Li^+} of $Li_4Ti_5O_{12}$ is about 10^{-11}–10^{-13} cm^2 s^{-1}, which agrees with earlier reports [19–23], while the D_{Li^+} of $SrLi_2Ti_6O_{14}$ is about 10^{-10}–10^{-11} cm^2 s^{-1}. In the middle of the charge or discharge process, the D_{Li^+} value of $SrLi_2Ti_6O_{14}$ is about one order of magnitude larger than that of $Li_4Ti_5O_{12}$.Thus, the Li migration resistance in the $SrLi_2Ti_6O_{14}$ lattice is smaller than that in the $Li_4Ti_5O_{12}$ lattice, even though both of them have 3D-networked structures. The high electronic conductivity and high Li migration capability in the $SrLi_2Ti_6O_{14}$ particles led to excellent power performance in the $LiCoO_2$/$SrLi_2Ti_6O_{14}$ batteries.

4. Conclusions

Li-ion batteries with 6 Ah capacities were designed and constructed for an HEV application, using $SrLi_2Ti_6O_{14}$ or $Li_4Ti_5O_{12}$ as the anode. Although the practical reversible capacity of $SrLi_2Ti_6O_{14}$ is lower than $Li_4Ti_5O_{12}$, $LiCoO_2$/$SrLi_2Ti_6O_{14}$ batteries had higher energy densities than the $LiCoO_2$/$Li_4Ti_5O_{12}$ batteries due to their higher operating voltages. Using the HPPC method to test the power characteristics of the batteries, the $LiCoO_2$/$SrLi_2Ti_6O_{14}$ batteries exhibited excellent power input and output performance, especially in charge power, achieving a 3973 W kg^{-1} specific charge power at 50% DOD. The outstanding power performance of the $LiCoO_2$/$SrLi_2Ti_6O_{14}$ batteries can be attributed to the higher Li-ion diffusion capability and higher electronic conductivity of $SrLi_2Ti_6O_{14}$ compared with $Li_4Ti_5O_{12}$.

Acknowledgments

This work was financially supported by the National High-Tech Research and Development (863) Plan of China (no. 2011AA11A230).

Appendix A. Supplementary data

Supplementary data related to this article can be found at http://dx.doi.org/10.1016/j.jpowsour.2013.06.149.

References

[1] T. Ohzuku, A. Ueda, N. Yamamoto, J. Electrochem. Soc. 142 (1995) 1431.
[2] Z. Yang, D. Choi, S. Kerisit, K.M. Rosso, D. Wang, J. Zhang, G. Graff, J. Liu, J. Power Sources 192 (2009) 588.
[3] H. Zhao, Y. Li, Z. Zhu, J. Lin, Z. Tian, R. Wang, Electrochim. Acta 53 (2008) 7079.
[4] R. Cai, A.S. Jiang, X. Yu, B. Zhao, H. Wang, Z. Shao, J. Mater. Chem. 22 (2012) 8013.
[5] D. Yoshikawa, Y. Kadoma, J.M. Kim, K. Ui, N. Kumagai, N. Kitamura, Y. Idemoto, Electrochim. Acta 55 (2010) 1872.
[6] T. Ogihara, M. Yamada, A. Fujita, S. Akao, K. Myoujin, Mater. Res. Bull. 46 (2011) 796.
[7] S.H. Ju, Y.C. Kang, J. Power Sources 189 (2009) 185.
[8] L. Kavan, M. Gratzel, J. Rathouský, A. Zukalb, J. Electrochem. Soc. 143 (1996) 394.
[9] D. Dambournet, I. Belharouak, K. Amine, Inorg. Chem. 49 (2010) 2822.
[10] I. Belharouak, K. Amine, Electrochem. Commun. 5 (2003) 435.
[11] D. Dambournet, I. Belharouak, J. Ma, K. Amine, J. Power Sources 196 (2011) 2871.
[12] Freedom CAR Battery Test Manual for Power Assist Hybrid Electric Vehicles, U.S. Department of Energy, October 2003. DOE/ID-11069.
[13] K.M. Shaju, G.V.S. Rao, B.V.R. Chowdari, Electrochim. Acta 49 (2004) 1565.
[14] X.H. Rui, N. Ding, J. Liu, C. Li, C.H. Chen, Electrochim. Acta 55 (2010) 2384.
[15] Z. Li, F. Du, X. Bie, D. Zhang, Y. Cai, X. Cui, C. Wang, G. Chen, Y. Wei, J. Phys. Chem. C 114 (2010) 22751.
[16] H. Yu, Y. Wang, D. Asakura, E. Hosono, T. Zhang, H. Zhou, RSC Adv. 2 (2012) 8797.
[17] K.M. Shaju, G.V. Subba Rao, B.V.R. Chowdari, Electrochim. Acta 48 (2003) 2691.
[18] E. Deiss, Electrochim. Acta 50 (2005) 2927.
[19] M. Wagemaker, R.H. Ernst, A. Kentgens, M.M. Fokko, J. Phys. Chem. B 113 (2009) 224.
[20] Y.Q. Wang, L. Gu, Y.G. Guo, H. Li, X.Q. He, S. Tsukimoto, Y. Ikuhara, L.J. Wan, J. Am. Chem. Soc. 134 (2012) 7874.
[21] C.Y. Ouyang, Z.Y. Zhong, M.S. Lei, Electrochem. Commun. 9 (2007) 1107.
[22] L. Kavan, J. Procházka, T.M. Spitler, M. Kalbáč, M.T. Zukalová, T. Drezen, M. Grätzel, J. Electrochem. Soc. 150 (2003) A1000.
[23] Y.H. Rho, K. Kanamura, J. Solid State Chem. 177 (2004) 2094.